Enhanced photoelectrocatalytic performance from size effects in pure and La-doped BiFeO$_3$ nanoparticles

Chuanfu Huang[1] · Xiaoli Zhang[1] · Heng Zhang[1] · Wei Zhang[1] · Changyong Lan[2] · Mingxue Li[1]

Abstract

Due to the energy crisis, the development of high-performance photoelectrocatalysts is becoming a hot research area in recent years. Among the materials studied, BiFeO$_3$ (BFO) exhibits excellent photoelectrocatalytic performance due to its moderate bandgap and unique band structure. In this paper, both pure BFO and La-doped BFO were synthesized by solgel method. The average size of the BFO nanoparticles was tuned from 65 to 440 nm. For the La-doped BFO, the average size of the nanoparticles was reduced from 95 to 40 nm with the increase in doping level from 0 to 30%. Next, the photoelectrocatalytic performance of the pure BFO nanoparticles were enhanced with the reduction in nanoparticle size, which was possibly caused by increased surface-to-volume ratio. For the increase in doping of La, the corresponding photoelectrocatalytic performance was first enhanced and then degraded. To understand the obtained results, a mechanism was proposed, which can be attributed to the competition between geometric size effects and surface effects. Our findings provided a controlled way to tune the photoelectrocatalytic performance of BFO system, which is crucial for practical applications.

Keywords BiFeO$_3$ nanoparticles · La-doped · Enhanced photoelectrocatalytic properties · Competition mechanism

1 Introduction

The development of high-performance photocatalysts is very important due to energy crisis and becomes a hot topic in recent years [1–4]. BFO, a single-phase multiferroic material that can be modified by doping other elements to acquire the improved ferroelectric and ferromagnetic properties [5–7], has also shown potential application in photoelectrocatalytic area because of its moderate bandgap (~ 2.3 eV) and unique band structure [8–10]. Until now, many researchers have investigated the photoelectrocatalytic properties of BFO

nanoparticles or films, but the low activity of BFO is still a big challenge [11–14]. In order to improve its photoelectrocatalytic property, various methods were used. For instance, Gu et al. inserted a layer of porous carbon into the BFO film and Pt catalyst and found the enhanced photocathodic performance [15]. In other aspects, to attain a satisfactory photocatalyst of BFO, one important way is to increase the surface area and reactivity with concurrently improving the absorption probability of photons and chemical reacting chances.

In this regard, numerous researches have focused on the photocatalytic performance of BFO-based nanoparticles that can increase the surface-to-volume area compared to films. For instance, a controlled hydrothermal method was applied to alter the morphologies for BFO particles, whose optical properties were strongly correlated with the particle size and shape [16]. In addition, researchers have found that hexagonal-shaped sillenite-type BFO nanoparticles (18–33 nm) owned higher photocatalytic activity compared to spherical perovskite-type BFO nanoparticles [17]. From the general idea, smaller-sized nanoparticles mean greater surface area and higher reactivity to ensure more pollutant molecules can be participated and decomposed [18, 19]. In other words, the reduction in BFO nanoparticle size can also possibly tune

✉ Chuanfu Huang
chuanfuh@cumt.edu.cn

✉ Mingxue Li
lmxueee@126.com

1 School of Materials Science and Physics, China University of Mining and Technology, Xuzhou 221116, Jiangsu, China

2 School of Optoelectronic Science and Engineering, University of Electronic Science and Technology of China, Sichuan 610054, China

its band structure, thus enhancing photocatalytic characteristics. However, the recent study has yielded the unexpected result that with the decreasing size of BFO nanoparticles, the depressed photocatalytic activity was observed and the possible mechanism was discussed based on the skin layer of BFO, which may bring some defects and local distortions that will result in low light absorption efficiency [20].

Apart from the above researches, it is generally known that ion doping can play an effective role in the improvement of the photocatalytic characteristics. For example, various ions, such as La, Sm, Mn, Ce, Co, Gd, and Ni, were doped or co-doped into BFO nanoparticles to acquire enhanced photocatalytic activities [9, 21–27]. However, we found that pursuing a reproducible method for synthesizing of La-doped BFO is still a challenge, e.g., the prepared La-doped BFO particles existed in impure phases in the studies [21, 22]. Moreover, to our best knowledge, there are seldom researches worked on the photoelectrocatalytic properties of the pure or La-doped BFO nanoparticles. Here, we report the successful preparation of a series of pure and La-doped BFO nanoparticles of different sizes (~ 40 nm to ~ 400 nm) without impure phases. Basically, the size was manipulated by the control of annealed temperature and the level of lanthanum doping. Differently, the outcome in our work is that with the reduction in pure BFO nanoparticle size, the overall photocatalytic activity exhibited an enhancement. In addition, with the increase in doping of La, the photoelectrocatalytic performance first enhanced and then degraded. The possible mechanism is discussed and from our perspective, we believe that there existed a certain competition mechanism between the altered structure, skin layer effect [28], and large surface area of the prepared nanoparticle samples of this research.

2 Experimental section

2.1 BiFeO$_3$ and La-doped BiFeO$_3$ nanoparticle preparation

The solgel method was used to synthesize pure BFO nanoparticles with the following procedure: The reactants of bismuth nitrate [Bi(NO$_3$)$_3$·5H$_2$O] and ferric nitrate [Fe(NO$_3$)$_3$·9H$_2$O] were weighed based on the stoichiometric ratio of Bi/Fe = 1:1 and subsequently dissolved in dilute nitric acid, with the attained mixed solution stirred at room temperature for 40–60 min until it was completely dissolved. Next, the chelating agent tartaric acid was added to the solution and the metering ratio was the same as that of Bi or Fe. The solution was stirred at 50 to 60 °C for an additional 60 min, with the color of the solution observed to be a pale-yellow sol. The prepared sol solution was thoroughly dried in an oil bath at 150 °C, which means a dry powder of BFO

gel can be attained. For this work, a series of BFO gel powder samples were annealed in a furnace for 2 h to obtain pure crystalized BFO nanoparticles at different calcination temperatures, including $T = 450$ °C, 500 °C, 550 °C, 600 °C, and 650 °C. It should be emphasized that all samples were held at 300 °C for 1 h to remove organic components during the process of heating up.

Similarly, Bi$_{1-x}$La$_x$FeO$_3$ ($x = 0.1$ to 0.3) nanoparticles were prepared according to a similar process for synthesizing of pure BFO nanoparticles. The difference is that the annealing temperature of Bi$_{1-x}$La$_x$FeO$_3$ nanoparticles was only maintained at 500 °C for 2 h, and the stoichiometric ratio of Bi/La/Fe = $(1 - x):x:1$. Correspondingly, the amounts were weighted for bismuth nitrate [Bi(NO$_3$)$_3$·5H$_2$O], iron nitrate [Fe(NO$_3$)$_3$·9H$_2$O], and lanthanum nitrate [La(NO$_3$)$_3$·6H$_2$O].

2.2 Characterization and photoelectrocatalytic performance measurements

The crystal structures of the synthesized nanoparticles were characterized by X-ray diffractometer (Bruker D8 Advance) with Cu Kα ($\lambda = 1.5418$ Å) radiation. The morphologies of the nanoparticles were detected by a field-emission scanning electron microscope (Hitachi SU8220). To measure the UV–Vis absorption spectra of the series of BFO nanoparticles, the ethylene glycol monomethyl ether and the samples dispersed in the ethylene glycol monomethyl ether were separately put into the cuvettes and then detected by a dual-beam UV–Vis spectrophotometer (Persee, TU-1901). The photoelectrocatalytic activity was assessed by an electrochemical workstation (Chenhua, CHI660E) with a solar simulator (Sanyou, SS-50A, 100 mW cm^{-2}). The workstation configuration was as follows: 1 mol/L NaOH solution was applied as the electrolyte (PH = 14), the Pt/Ti/SiO$_2$/Si substrate for mounting samples was employed as the working electrode, the counter electrode was a Pt foil, and the reference electrode was Ag/AgCl.

3 Results and discussion

3.1 Crystal structure of pure and La-doped BiFeO$_3$ nanoparticles

Before carrying out photoelectrocatlytic measurements, it is necessary to check the phase purity of the as-synthesized nanoparticles that are easy to form purity phases in the synthesis of BFO. The X-ray diffraction (XRD) patterns of the as-synthesized nanoparticles are shown in Fig. 1. As can be seen from Fig. 1a, the samples without doping are pure phase BFO, and all the diffraction peaks can be indexed according to *R3c* BFO (JCPDS No. 86-1518). It can be found that the annealing temperature did not affect the phase purity
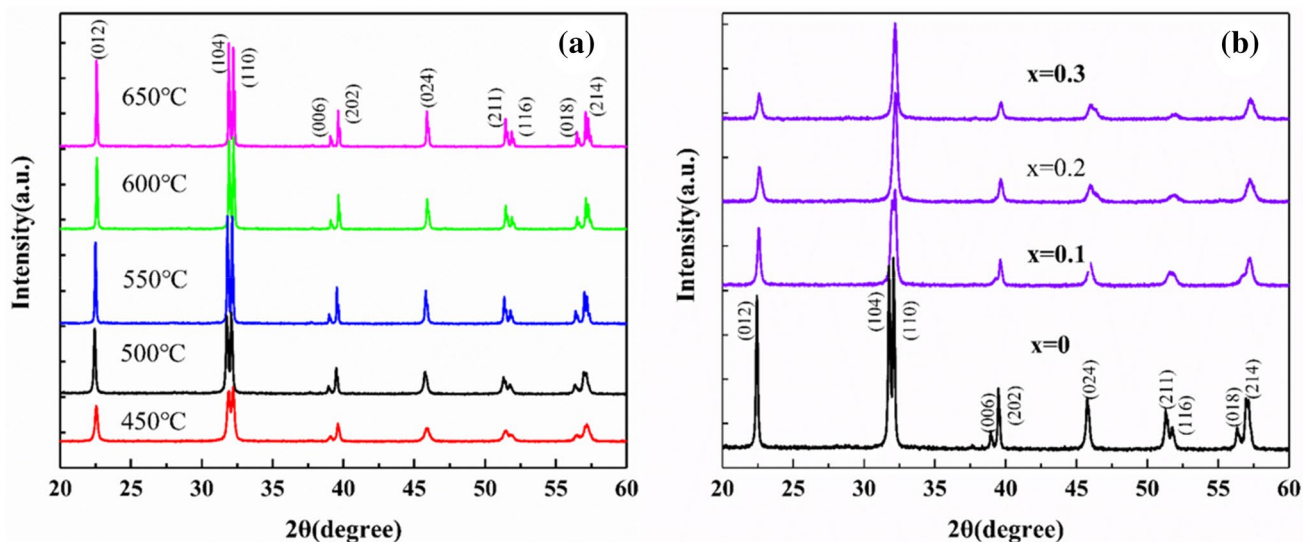
Fig. 1 XRD patterns of **a** BFO nanoparticles prepared at the different annealed temperatures (from 450 to 650 °C) and **b** $Bi_{1-x}La_xFeO_3$ nanoparticles with the doping level x from 0 to 0.3
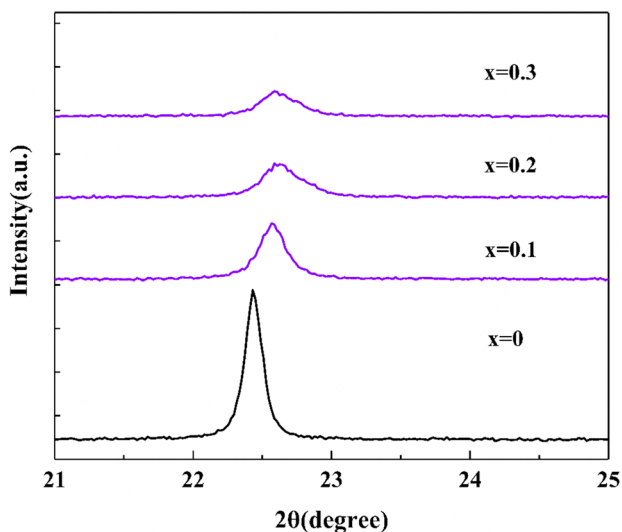

Fig. 2 XRD patterns for Fig. 1b near the diffraction angle $2\theta = 22.5°$, and it can be found that the full width at half maximum will be expanded with the increasing value of x. From the Scherrer formula, we can expect that the size of La-doped BFO nanoparticle will be reduced with the increase of doping level x

of the samples. For the La-doped samples, phase transition can be observed for the BFO crystal structure. Specifically, with the increase in the doping level of La, the phase was changed from the distorted rhombohedral *R3c* to tetragonal phase because the peaks of [(104), (110)] and [(108), (214)] emerged into single peaks of [(208)] and [(220)].

Figure 2 indicates the magnification XRD pattern near diffraction angle of 22.5° in Fig. 1b, the average size of the La-doped BFO nanoparticles can be estimated according to the Scherrer formula, and the size was ~70 nm, ~41 nm, ~28 nm, and ~23 nm corresponding to the doping level from $x = 0$ to $x = 0.3$. Although this estimation might be inaccurate, it can definitely demonstrate that with the increase in La doping level, the BFO nanoparticle size will be reduced. Next, we will employ the field-emission scanning emission electron microscopy (FE-SEM) to more straightly observe the size of nanoparticles.

3.2 Morphology of BFO nanoparticles

We believe that the size of the BFO nanoparticles is an important parameter for photoelectrocatalytic performance. This way, the morphologies of the as-synthesized products were checked by the FE-SEM images of the undoped BFO, as shown in Fig. 3. It can be clearly seen that the size of pure BFO nanoparticles increased with the increase in annealing temperature (450–650°C), which should be due to the increased kinetic energy at high temperatures. To obtain the average size of those pure BFO nanoparticles, the number of nanoparticles was statistically accounted at different sizes, and the corresponding size distribution histograms are drawn in supporting information Figure S1. The average size increased from 65 to 440 nm as shown in Fig. 3f. Moreover, for the annealed temperatures of 550 °C to 650 °C in Fig. 3c–e, the nanoparticle size dramatically increased, with the large size fluctuation. For Fig. 3c, the shape of BFO nanoparticles was more like disk, while for Fig. 3e, the BFO nanoparticles were formed as microcrystals with the clear edges and corners. Consequently, it can be seen that with our experimental conditions, the size of the prepared BFO
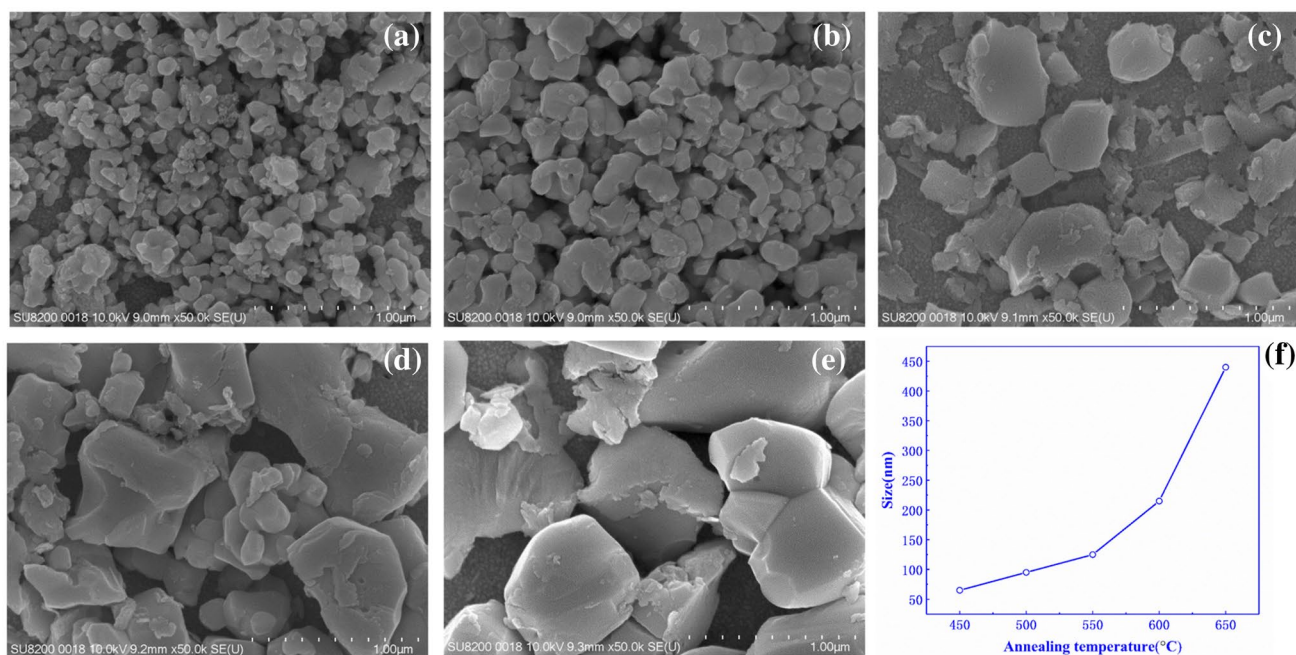
Fig. 3 **a–e** The FE-SEM graphs for pure BFO nanoparticles annealed from 450 to 650 °C, and **f** summarizes their average size versus annealing temperature

nanoparticles were much larger than the size of the BFO nanoparticles obtained in other research groups [16, 20].

To further reduce the size of the BFO nanoparticles, lanthanum with different concentrations was doped into BFO samples. For those La-doped BFO nanoparticles, their morphologies can be clearly seen from FE-SEM images shown in Fig. 4a–c. Similarly, to more accurately describe the doped particle information, the histograms of particle size distribution were drawn in the supporting information Figure S2. Also, we can get the average size for La-doped BFO nanoparticles as ~ 95 nm, ~ 55 nm, ~ 50 nm, and ~ 40 nm when the concentration of La doping level was increased from 0 to 30%. Specifically, when the concentration of La doping level was 10% for the BFO sample, we can see that the overall nanoparticles were well separated and the size distribution was also more uniform compared to the undoped BFO nanoparticles, as shown in Fig. 4a. Moreover, the average nanoparticle size was reduced from ~ 95 to ~ 55 nm, with the size range of ~ ± 10 nm. With the increase in La doping level to 20% concentration, the BFO nanoparticle size will be continuously lowered to a smaller size, which is around 50 nm, and it can be found that there existed certain agglomerates, which displayed the disk or island shape that consisted of nanoparticles. This phenomenon will be more severe when the doping concentration was to 30% as shown in Fig. 4c, and it can be explained by further reduction in size of nanoparticles, thus leading to the self-assemble or agglomerate phenomenon (disk or island). In Fig. 4d, it can be found that the smallest nanoparticle size was near ~ 40 nm, but in

other way, the agglomerate will be more dominant. Thus, it can be concluded that with the doping level increase, the BFO nanoparticle size will be correspondingly decreased, but it also can bring the nanoparticle agglomeration, which might affect the photoelectrocatalytic characteristics of BFO nanoparticles.

3.3 Photoelectroactivity of BiFeO$_3$ nanoparticles

Now let us concentrate on the photoelectrocatalytic performance of the prepared nanoparticles, and we first measured those nanoparticle photocurrents using a chemical workstation with a sun simulator(100 mW/cm^2), as shown in Fig. 5a–d. Specifically, the applied voltage was from 0 to 0.6 V, which can be represented as $V_{Ag/AgCl}$ and be transferred to a reversible hydrogen potential (RHE) scale, with the formula of $V_{RHE} = V_{Ag/AgCl} + 0.2224$ V $+ 0.059 \times$ PH, where V_{RHE} was the potential versus the reversible hydrogen potential, $V_{Ag/AgCl}$ was the potential versus Ag/AgCl electrode, and pH value was equal to 14, from an aqueous solution of 1 M NaOH. It can be seen in Fig. 5a that for different sizes of pure BFO nanoparticles, with the reduction in nanoparticle size, the photocurrents, which can directly reflect the photoelectrocatalytic activity, were overall increased except for the nanoparticle size of ~ 65 nm. This also can be more explicitly demonstrated in Fig. 5b, which lists the photocurrent values with different nanoparticle size when the RHE potential was 1.5 V. Thus, it can be found that when the nanoparticle was near ~ 95 nm, it
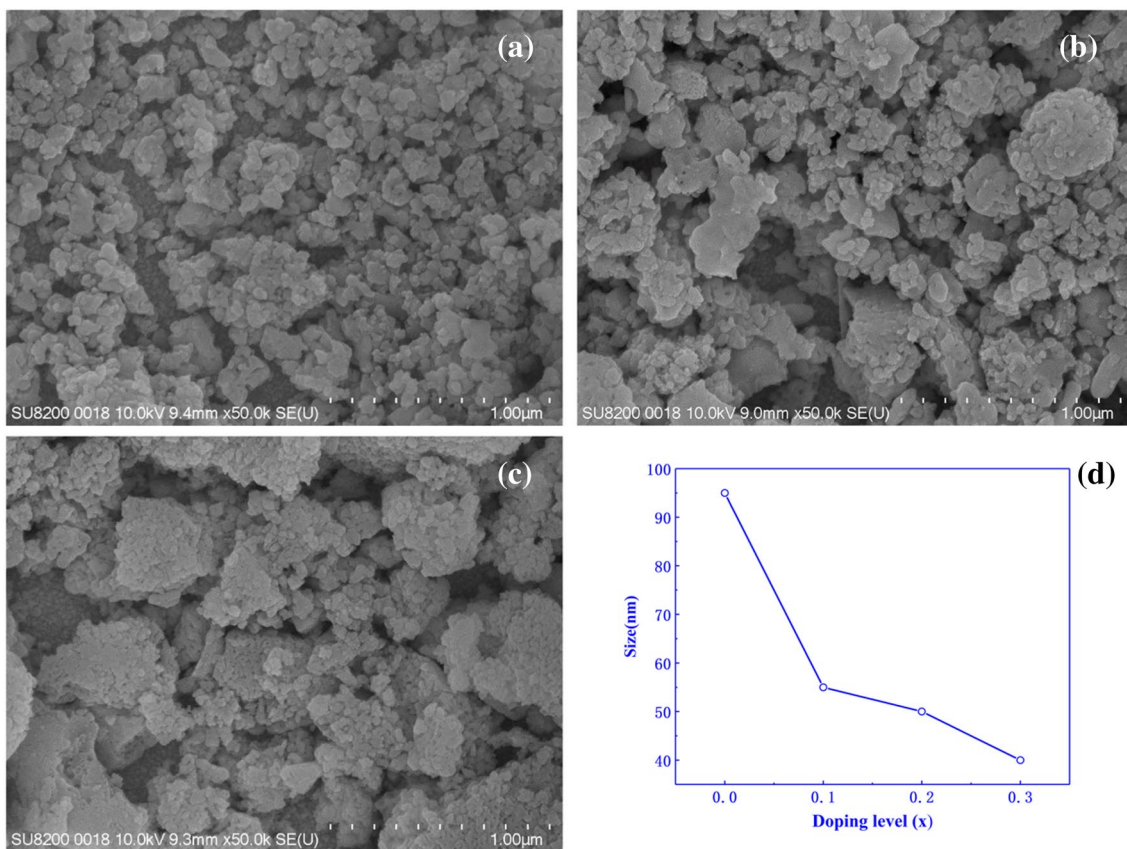
Fig. 4 **a–c** Exhibits the FE-SEM pictures for La-doped BFO nanoparticles with the doping level from 10 to 30%, and **d** shows the relationship between the particle average size and doping level *x*

had the optimum photoelectrocatalytic activity. Here, the photoelectron catalytic performances followed the principle that a good catalyst should have a larger surface area, which can enhance the reactivity possibility for absorption of photons assurance an effective charge transfer to the adjacent reactants for oxidation–reduction processes. However, it can be seen that the photoelectrocatalytic efficiency of ~ 65 nm BFO nanoparticles was slightly lower than that of ~ 95 nm nanoparticles, and it is possibly due to existence of certain particle agglomerations that will reduce the surface area, as shown in Fig. 3a.

Thus, based on the findings from Fig. 5c, we eventually chose the temperature of 500 °C as the annealed temperature for all La-doped BFO nanoparticles, which can be considered as the optimal experimental temperature condition. For Fig. 5c, it can be found that with the different doping levels of La, the photocurrents were also correspondingly altered. Moreover, we found that when the La doping level was 20%, the photoelectrocatalytic performance was most active, and this can be clearer seen from the photocurrents of La-doped samples that demonstrated in Fig. 5d with the RHE potential at 1.5 V. Similarly, the threshold potential was near 1.37 V.

Here, it is suitable to make some conclusions that with the reduced size of pure BFO nanoparticles, the photoelectrocatalytic performance was overall increased except for the pure BFO nanoparticles prepared at the annealed temperature of 500 °C. Furthermore, for those La-doped BFO nanoparticles, they will own much higher photoelectrocatalytic activity than that of the pure BFO nanoparticles, e.g., when the doping level of *x* = 0 to 0.2, the activity of photoelectrocatalysis was increased, whereas when *x* increased from 0.2 to 0.3, the photoelectrocatalytic activity will be decreased. It can be found one interesting phenomenon that for pure or doped BFO nanoparticles, both of them had certain turning points for photoelectrocatalytic activity, which seemed having a strong relationship with nanoparticle size but this relationship was not linear. Obviously, our results were different from the outcomes in the previous research, which demonstrated that with the reduction in pure BFO nanoparticles in the range from ~ 30 to ~ 190 nm, their photocatalytic performance will be correspondingly reduced [17]. Although Ref. 17 focused on the photocatalytic characteristics of pure BFO nanoparticles, it still can give us certain guidance to explain our outcome. We will attempt to figure out the experimental fact in the following sections.
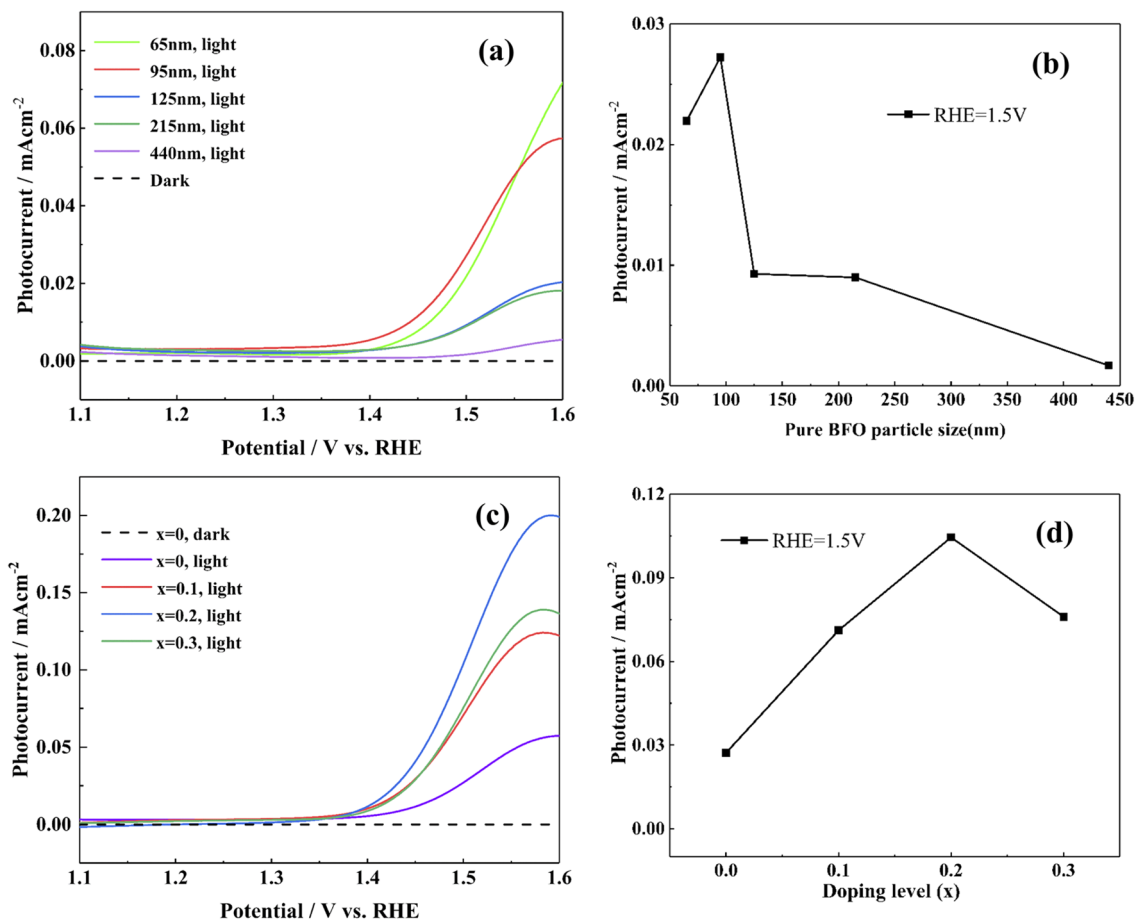
Fig. 5 **a**, **c** The photocurrent–potential curves of the pure and La-doped BFO nanoparticles. **b**, **d** are given the photocurrents of particle samples with the different size of pure BFO and the dissimilar dop-ing level of doped BFO at 1.5 V versus RHE, respectively. Electrolyte was 1 M NaOH, and the power of light source was 100 mW/cm^2 from a sunlight simulator

3.4 Mechanism of photoelectroactivity of BiFeO$_3$ nanoparticles

The photoelectrocatalytic performance is dependent on many factors, and one of the significant factors is the band gap that can strongly affect the photoelectrocatalytic characteristics. To acquire more insights of the obtained photoelectrocatalytic results, basically, we collected the UV–Vis spectra of the pure and La-doped nanoparticles, as shown Fig. 6. Figure 6a shows the UV–Vis spectra from 300 to 800 nm for the pure BFO nanoparticles prepared at different temperatures, and the spectra exhibited the complicated curves due to the complex of BFO band structure. Next, the Kubelka–Munk theory was employed to estimate the band gaps of the pure BFO nanoparticles, and the absorption coefficient α, photon energy $h\nu$, and band gap E_g have the following relationship:

$$(\alpha h \nu) = A\left(h\nu - E_g\right)^{\frac{1}{2}},$$

where h is the Planck constant and A is a constant function. The corresponding energy gaps can be attained by extrapolating the linear portion of $(\alpha h\nu)^2$ to zero, as demonstrated in the inset of Fig. 6a. Thus, the energy gaps of pure BFO nanoparticles from 65 to 440 nm are approximately to 2.21 eV, 2.13 eV, 2.27 eV, 2.38 eV, and 2.59 eV, respectively. It can be seen that the attained energy band gaps for the nanoparticle size smaller than 150 nm were consistent with the previous researches [29, 30], and also it can be found that the nanoparticles prepared at ~ 95 nm owned the smallest energy band gap.

For Fig. 6b, it indicates that the UV–Vis spectra were collected from 300 to 800 nm for La-doped BFO nanoparticles with the doping level from 0 to 30%. Similarly, with the Kubelka–Munk theory, the energy gaps can be estimated as 2.13 eV, 2.46 eV, 2.43 eV, and 2.67 eV that correspond to the La-doped BFO nanoparticles with the doping level from $x=0$ to $x=0.3$. It can be concluded with the increasing La doping level, the energy gap was also overall increased, and this seems conflicting with the previous research [21]. For
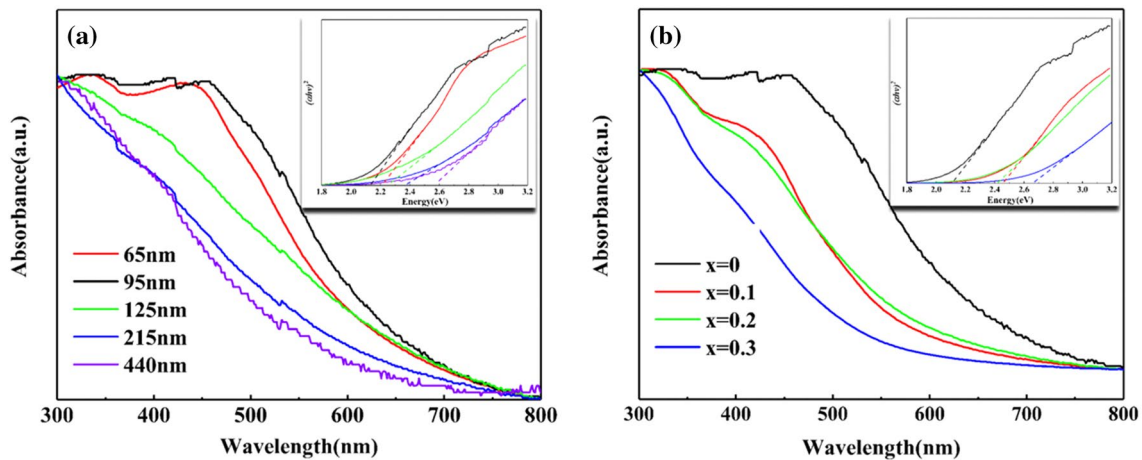
Fig. 6 UV–Vis spectra from 300 to 800 nm **a** for pure BFO nanoparticles, **b** for doped BFO nanoparticles

the doping level $x=0.2$, the doped BFO nanoparticles owned the smallest energy gap.

From the above experimental results, it can be seen that there are main three factors including the crystal phase, nanoparticle size, and the energy gap, which can strongly impact the photoelectrocatalytic performance of pure and La-doped BFO nanoparticles. For instance, with the decrease in pure nanoparticle BFO samples, it can be possibly concluded that the photoelectrocatalytic performance will be also increased, as shown in Fig. 5a, b. This also can be verified from the experimental findings for the La-doped BFO samples, as demonstrated in Fig. 5c, d. However, as the La doping level increased, it should not be neglected for one fact that the phase structure will be gradually changed. For the reduction in nanoparticle size and phase transition, both of them can be attributed to "geometric size effects" based on our understanding [19]. These effects include two aspects: First, the smaller size of nanoparticles can enhance the surface-to-volume ratios and thus will correspondingly enlarge the densities of catalytically active sites. Second, the size reduction will influence or disturb the intrinsic electronic and lattice structure of the particles. Eventually, the band gap structure of the nanoparticle samples will be also perturbed, and this physical picture can also be observed by other researches [18, 19]. Now it might be confidently concluded that the "geometric size effects" are dominant in the pure and doped BFO nanoparticles, and with the reduction in geometric size of nanoparticles, the corresponding photoelectrocatalytic properties will also be improved.

However, we should not ignore the facts that for ~95-nm pure BFO nanoparticles or the BFO nanoparticles with La doping level x = 0.3, although they had the smallest size in the pure or doped sample groups, they did not own the strongest photoelectrocatalytic performance. It should be also noticed that when the nanoparticle size was lowered,

the agglomeration will be also more severe, as demonstrated by Figs. 3a and 4c which will reduce the dominance of "geometric size effects." Thus, the photoelectrocatalytic performance will also be affected. Last, one more factor that might have influenced the photoelectrocatalytic activity is the skin layer that is inherent to oxides like BFO, which can modify the optical response due to the defects and local distortions located at the sample surface. Thus, the two factors of agglomeration and skin layer will strongly lower the photoelectrocatalytic performance of BFO nanoparticles, which can be attributed as "surface effects" that will reduce the effective chemical reacting surface area, thus lowering the photoelectrocatalytic activity of prepared BFO nanoparticles.

To more profoundly understand the experimental fact in this paper, we proposed a new mechanism that there possibly existed certain competition between geometric size effects and surface effects of the pure or La-doped BFO nanoparticles, and the proposed mechanism is the critical part in this paper, as demonstrated in Fig. 7. The first effects will increase the reactivity possibility between the molecules and catalysis, while the second effects will bring uncertain defects or overlaps of the nanoparticles that could impact or lower the photoelectrocatalytic activities. In other words, it was because of the competition mechanism causing the phenomenon of having turning points for photoelectrocatalytic activities in Figs. 5b, d. More specifically, when the BFO nanoparticles were in the small size scale, both geometric size effects and surface effects will be dominant due to the large surface-to-volume ratios, but they will play an opposite function on the photoelectrocatalytic performance for the BFO nanoparticles in this work. Since these factors are relatively complex, we believe more researches should be required to clarify this new mechanism to acquire more insights of the behind mechanism.
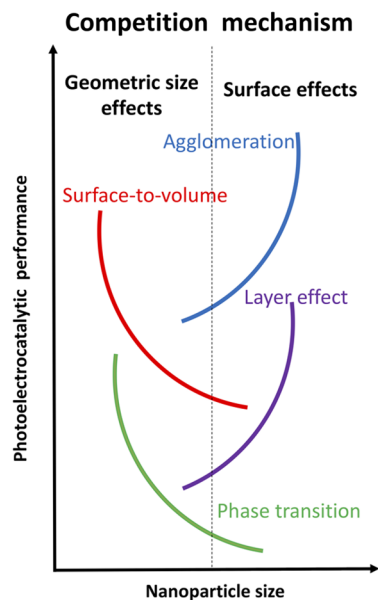
Competition mechanism

Fig. 7 A new perspective was proposed in this paper, and there possibly existed the competition mechanism between geometric size effects and surface effects of the prepared BFO particles. Correspondingly, geometric size effects (increasing surface-to-volume and phase transition) will be attained with the reduction of particle size, and these effects will enhance the photoelectrocatalytic performance of the particles. Conversely, with the particle size decreasing, surface effects (bringing the agglomeration and layer effect) will disturb the photoelectrocatalytic performance of the nanoparticles

4 Conclusion

In this paper, the photoelectrocatalytic performance was investigated for pure $BiFeO_3$ (BFO) and $Bi_{1-x}La_xFeO_3$ nanoparticles ($x = 0, 0.1, 0.2, 0.3$), which were prepared successfully without impurities. For pure BFO nanoparticles, the nanoparticle size from ~65 to 440 nm were synthesized, while the La-doped BFO nanoparticle size reduced from ~95 to 40 nm as the doping level of x was increased from 0 to 0.3. From the experimental results, it can be seen that with the decreasing size of pure BFO nanoparticles, the photoelectrocatalytic performance of these nanoparticles also will be enhanced. While for the La-doped BFO nanoparticles, they will have noticeably increased photoelectrocatalytic performance compared to the pure BFO nanoparticles. From our analysis, the increased photoelectrocatalytic activity was attributed to geometric size effects, which might be simultaneously perturbed by surface effects from the nanoparticle agglomeration and skin layer of BFO nanoparticles. In other words, a new competition mechanism between the altered structure, skin layer effect [25] and large surface area of the prepared nanoparticles was proposed for this research, and the new findings provided a possible approach to control the photoelectrocatalytic performance of BFO system, which is crucial for practical applications.

Compliance with ethical standards

Conflict of interest The authors declare no competing conflict of interest.

References

1. J.A. Turner, Sustainable hydrogen production. Science **305**, 972–974 (2004)
2. T.W. Kim, K.-S. Choi, Nanoporous $BiVO_4$ photoanodes with dual-layer oxygen evolution catalysts for solar water splitting. Science **343**, 1245026 (2014)
3. C.R. Jiang, S.J.A. Moniz, A.Q. Wang, T. Zhang, J.W. Tang, Photoelectrochemical devices for solar water splitting-materials and challenges. Chem. Soc. Rev. **46**, 4645–4660 (2017)
4. J. Kreisel, M. Alexe, P.A.A. Thomas, Photoferroelectric material is more than the sum of its parts. Nat. Mater. **11**, 260 (2012)
5. W.Y. Xing, Y. Ma, Z. Ma, Y.L. Bai, J.Y. Chen, S.F. Zhao, Improved ferroelectric and leakage current properties of Er-doped $BiFeO_3$ thin films derived from structural transformation. Smart Mater. Struct. **23**, 8 (2014)
6. Q. Yun, Y.L. Bai, J.Y. Chen, W. Gao, A. Bai, S.F. Zhao, Improved ferroelectric and fatigue properties in Ho doped $BiFeO_3$ thin films. Mater. Lett. **129**, 166 (2014)
7. C.F. Huang, Structural and magnetic characterization of $Bi_{1-x}La_xFeO_3$ and $BiFe_{1-y}Mn_yO_3$ nanoparticles synthesized via a sol–gel method. Phase Transit. **92**, 2 (2019)
8. T. Choi, S. Lee, Y.J. Choi, V. Kiryukhin, S.W. Cheong, Switchable ferroelectric diode and photovoltaic effect in $BiFeO_3$. Science **324**, 63–66 (2009)
9. N. Zhang, D. Chen, F. Niu, S. Wang, L.S. Qin, Y.X. Huang, Enhanced visible light photocatalytic activity of Gd-doped $BiFeO_3$ nanoparticles and mechanism insight. Sci. Rep. **6**, 26467 (2016)
10. P. Yilmaz, D. Yeo, H. Chang, L. Loh, S. Dunn, Perovskite $BiFeO_3$ thin film photocathode performance with visible light activity. Nanotechnology **27**, 345402 (2016)
11. S.M. Lam, J.-C. Sin, A.R. Mohamed, A newly emerging visible light-responsive $BiFeO_3$ perovskite for photocatalytic applications: a mini review. Mater. Res. Bull. **90**, 15–30 (2017)
12. J. Song, T.L. Kim, J. Lee, S.Y. Cho, J. Cha, Y.S. Jeong, H. An, W.S. Kim, Y.-S. Jung, J. Park, Y.G. Jung, D.-Y. Kim, J.Y. Jo, S.D. Bu, H.W. Jang, S. Lee, Domain-engineered $BiFeO_3$ thin-film photoanodes for highly enhanced ferroelectric solar water splitting. Nano Res. **11**, 642–655 (2018)
13. C.R. Jiang, S.J.A. Moniz, A.Q. Wang, T. Zhang, J.W. Junwang Tang, Photoelectrochemical devices for solar water splitting—materials and challenges. Chem. Soc. Rev. **46**, 4645–4660 (2017)
14. I. Papadas, J.A. Christodoulides, G. Kioseoglou, G.S. Armatas, A high surface area ordered mesoporous $BiFeO_3$ semiconductor with efficient water oxidation activity. J. Mater. Chem. A **3**, 1587–1593 (2015)
15. S.L. Gu, X.X. Zhou, F.G. Zheng, L. Fang, W. Dong, M.R. Shen, Improved photocathodic performance in Pt catalyzed ferroelectric $BiFeO_3$ films sandwiched by a porous carbon layer. Chem. Commun. **53**, 7052–7055 (2017)

16. S. Li, Y.H. Lin, B.P. Zhang, Y. Wang, C.W. Nan, Controlled fabrication of BiFeO$_3$ uniform microcrystals and their magnetic and photocatalytic behaviors. J. Phys. Chem. C **114**, 2903–2908 (2010)

17. X.H. Zhu, Q.M. Hang, Z.B. Xing, Y. Yang, J.M. Zhu, Z.G. Liu, N.B. Ming, P. Zhou, Y. Song, Z.S. Li, T. Yu, Z.G. Zou, Microwave hydrothermal synthesis, structural characterization, and visible-light photocatalytic activities of single-crystalline bismuth ferric nanocrystals. J. Am. Ceram. Soc. **94**, 2688–2693 (2011)

18. M. Khojasteh, S. Haghighat, J.M. Dawlaty, V.V. Kresin, Controlled deposition of size-selected MnO nanoparticle thin films for water splitting applications: reduction of onset potential with particle size. Nanotechnology **29**, 21 (2018)

19. Y. Li, A.I. Frenkel, Metal nanocatalysts, in *XAFS techniques for catalysts, nanomaterials, and surfaces, chapter19*, ed. by Y. Iwasawa, K. Asakura, M. Tada (Springer, Cham, 2017), pp. 273–298

20. X.F. Bai, J. Wei, B.B. Tian, Y. Liu, T. Reiss, N. Guiblin, P. Gemeiner, B. Dkhil, I.C. Infante, Size effect on optical and photocatalytic properties in BiFeO$_3$ nanoparticles. J. Phys. Chem. C **120**, 3595–3601 (2016)

21. R. Dhanalakshmi, M. Muneeswaran, K. Shalini, N.V. Giridharan, Enhanced photocatalytic activity of La-substituted BiFeO$_3$ nanostructures on the degradation of phenol red. Mater. Lett. **165**, 205–209 (2016)

22. W.W. Meng, R.S. Hu, J. Yang, Du Yanfei, J.J. Li, H.Y. Wang, Influence of lanthanum-doping on photocatalytic properties of BiFeO$_3$ for phenol degradation. Chin J. Catal. **37**, 1283–1292 (2016)

23. P.R. Vanga, R.V. Mangalaraja, M. Ashok, Structural, magnetic and photocatalytic properties of La and alkaline co-doped BiFeO$_3$ nanoparticles. Mater. Sci. Semicon. Proc. **40**, 796–802 (2015)

24. Z.J. Hu, D. Chen, S. Wang, N. Zhang, L.S. Qin, Y.X. Huang, Facile synthesis of Sm-doped BiFeO$_3$ nanoparticles for enhanced visible light photocatalytic performance. Mater. Sci. Eng. B **220**, 1–12 (2017)

25. S. Irfan, Y. Shen, S. Rizwan, H.-C. Wang, S.B. Khan, C.-W. Nan, Band-gap engineering and enhanced photocatalytic activity of Sm and Mn doped BiFeO$_3$ nanoparticles. J. Am. Ceram. Soc. **100**, 31–40 (2017)

26. J. Sharma, D. Basandrai, A.K. Srivastava, Ce-Co-doped BiFeO$_3$ multiferroic for optoelectronic and photovoltaic applications. Chin. Phys. B **26**, 116201 (2017)

27. M. Nadeem, W. Khan, S. Khan, M. Shoeb, S. Husain, M. Mobin, Significant enhancement in photocatalytic performance of Ni doped BiFeO$_3$ nanoparticles. Mater. Res. Express. **5**, 6 (2018)

28. X. Mart, P. Ferrer, J. Herrero-Albillos, J. Narvaez, V. Holy, N. Barrett, M. Alexe, G. Catalan, Skin layer of BiFeO$_3$ single crystals. Phys. Rev. Lett. **106**, 236101 (2011)

29. M.A. Basith, N. Yesmin, R. Hossain, Low temperature synthesis of BiFeO3 nanoparticles with enhanced magnetization and promising photocatalytic performance in dye degradation and hydrogen evolution. RSC Adv. **8**, 29613 (2018)

30. L.F. Fei, J.K. Yuan, Y.M. Hu, C.Z. Wu, J.L. Wang, Y. Wang, Visible light responsive perovskite BiFeO$_3$ pills and rods with dominant {111}c facets. Cryst. Growth Des. **11**, 1049–1053 (2011)